The binding process of BmKTX and BmKTX-D33H toward to Kv1.3 channel: a molecular dynamics simulation study

Qiancheng Zheng[1], Risong Na[2], Lianjuan Yang[3], Hui Yu[4], Xi Zhao[1*]and Xuri Huang[1*]

1. Laboratory of Theoretical and Computational Chemistry, Institute of Theoretical Chemistry, Jilin University, Changchun, China

2. College of plant protection, Henan Agricultural University, Zhengzhou, Henan, 45002, P.R China

3. Department of Mycology, Shanghai Dermatology Hospital, Shanghai, China

4. College of Science, Beihua Univesrity, Jilin, China

Acknowledgements

Abstract

The potassium channel Kv1.3 is an important pharmacological target and the Kaliotoxin-type toxins (α-KTX-3 family) are its specific blockers. Here, we study the binding process of two kinds of Kaliotoxin-type toxins:BmKTX and its mutant (BmKTX-D33H) toward to Kv1.3 channel using MD simulation and umbrella sampling simulation, respectively. The calculated binding free energies are -27 kcal/mol and -34 kcal/mol for BmKTX and BmKTX-D33H, respectively, which are consistent with experimental results. The further analysis indicate that the characteristic of electrostatic potential of the α-KTX-3 have important effect on their binding modes with Kv1.3 channel; the residue 33 in BmKTX and BmKTX-D33H plays a key role in determine their binding orientations toward to Kv1.3 channel; when residue 33(or 34) has negative electrostatic potential, the anti-parallel β-sheet domain of α-KTX-3 toxin peptide will keep away from the filter region of Kv1.3 channel, as BmKTX; when residue 33(or 34) has positive electrostatic potential, the anti-parallel β-sheet domain of α-KTX-3 toxin peptide will interact with the filter region of Kv1.3 channel, as BmKTX-D33H. Above all, electrostatic potential differences on toxin surfaces and correlations motions within the toxins will determine the toxin-potassium channel interaction model. In addition, the hydrogen bond interaction is the pivotal factor for the Kv1.3- Kaliotoxin association.

Understanding the binding mechanism of toxin–potassium channel will facilitate the rational development of new toxin analogue.

Keyword: MD simulation, umbrella sampling simulation, Kv1.3 channel, α-KTX-3 toxin, BmKTX, BmKTX-D33H, electrostatic potential, hydrogen bond.

1.Introduction

Effector memory T-cell (T_{EM}) is assumed to play a crucial role in the pathogenesis autoimmune disease, such as multiple sclerosis, type 1 diabetes, rheumatoid arthritis, psoriasis and chronic graft-versus host disease[1] . It has been proved that activated T_{EM} will increase Kv1.3 expression and the protein will be the dominant channel in T_{EM}[2]. The Kv1.3 channel as a member of voltage-dependent K+ channel family plays a critical role in effector memory T-cell, so it always is an important drug target.[3] Kv1.3 blockers potently inhibit calcium signaling, proliferation and cytokine secretion in autoreactive T_{EM} cells[4] .

There are evidences for scorpion toxin efficiently treat on different animal models of autoimmune diseases, such as ShK-Dap22[5], PAP-1[6]，BmKTX-D33H[7], MgTX[8]. Scorpion toxins have been classified with several structurally distinct families of peptidyl modulators of ion channels[9]. The α-KTX family classified from scorpion toxins that comprises short-chain (37–39 amino acids) with three disulfide bridges and can block potassium channel. Kaliotoxin-type subfamily 3 (α-KTX-3) which belong to α-KTX family, comprises one α-helix domain and two anti-parallel β-sheets and have been identified as potent blockers of Kv1.3[10-12]. Especially, the α-KTX-3 toxins have potent and selectively inhibition toward to the Kv1.3 channels[9]. The basic residues are rich in the α-KTX-3 toxins so that they can form favorable electrostatic interactions with the outer vestibule of Kv1.3 which contains several rings of acidic residues. In previous research, the predicted model of α-KTX-3 toxin -

Kv1.3 channel indicates that the toxin usually used its anti-parallel β-sheet domain to interact with the outer vestibule of Kv1.3 and one conserved Lys26(27) act as a channel pore-blocking residue inserting into the selectivity filter of Kv1.3[13-17]. Note that, aligning the sequences of α-KTX-3 subfamily, it often appears that one residue located at same position have two different serial numbers: like Lys26 of BmKTX-D33H and Lys27 of KTX (shown in the **Figure** 1) and the model has been widely accepted. For example, ChTX(α-KTx-1.1), OSK1(α-KTx-3.7), AgTX(α-KTx-3.2), KTX(α-KTx-3.1), all adopt the mentioned above interaction mode with the potassium channels. But a new binding mode of native toxin BmKTX(α-KTX-3.6) toward to Kv1.3 channel has been reported that BmKTX use its turn motif locating between the α-helice domain and the β-sheet domain to block the selectivity filter of Kv1.3[18]. The researchers found Asp33 influence the channel blocking ability of conserved Lys26 in BmKTX using mutation experiments. When BmKTX-D33H mutants to BmKTX-D33H/K26N, the IC_{50} value increased over 698-fold; when BmKTX mutants to BmKTX-K26N, the IC_{50} value only increased over 60-fold. In this paper, we confirmed that there is stronger positive correlation motion between residue33 and the conserved Lys26 in BmKTX and BmKTX-D33H, and electrostatic potential differences on residue 33 of toxin will determine the interactions of the conserved Lys26 with Kv1.3 channel. And also, the researchers probed the novel interacting surface of BmKTX toward Kv1.3 channel using alanine-scanning mutagenesis method and build a binding model using the ZDOCK

program[19]. However, the atomic detail and mechanism how the acidic residues affect the toxin–potassium channel binding model are not clear enough.

In recent years, molecular simulations of toxin peptides with ion channels have attract people to understand their mechanism of action[20-25] . Here, we built two accurate binding models which are BmKTX and BmKTX-D33H binding with Kv1.3 channel and the umbrella sampling method was used to study the toxin–potassium channel binding process. Our results indicated that the acidic residue Asp33 of BmKTX not only produce a strong negative electrostatic potential in toxin's surface but also have a strong positive correlation motion with Lys26. For other members of α-KTX-3 toxin subfamily, we also found that there is a strong positive correlation motion between the residue 33(34) and the conserved Lys26(27) that means that residue 33(34) of the α-KTX-3 toxin subfamily is the key residue which can influence the toxin–potassium channel binding. Different toxin–potassium channel binding modes often means a variety of drug effects. Our study provides an exact explanation for the important functional role of toxin acidic residues in forming diverse toxin–potassium channel binding modes.

2.Method

2.1 Homology model and molecular docking.

Amino acid sequence of Kv1.3 channel was downloaded from the SWISS-PROT database (P22001) and the Swiss-Model[26] was used to homology modeling. The Kv1.2(PDB ID: 2A79) which have 93% sequence identity was used as the template to build the homology model of Kv1.3[27]. The BmKTX was obtained from RCSB (PDB ID:1BKT) and the BmKTX as template to build the BmKTX-D33H model. The HADDOCK server[28] was used to generate toxin–potassium channel binding modes.

2.2 Molecular dynamics.

All MD simulations are performed using GROMACS-4.6.7[29] . The GROMOS96 53a6 force field[30] and TIP3P water model[31]are used to describe the interatomic interactions. The Kv1.3 channel was embedded in a POPC bilayer[32] . The number of POPC molecular is 512. A rectangular simulation box, which is under periodic boundary conditions, was filled in a toxin-kv1.3 with POPC bilayer, TIP3P water and 0.15M NaCl. The size of the box is 13nm×13nm×14nm.The temperature is kept at average 300 K by using the Nose-Hoover method[33]. The pressure is kept at average 1 atm by using the Parrinello-Rahman method[34].

2.3 Umbrella sampling.

In this study, the steered molecular dynamics method and the WHAM tool is used to calculate the PMF[35]. When the two binding models are embedded in the POPC bilayer and the TIP3P water and 0.15M NaCl were added, the systems prepared

finally. Before umbrella sampling simulation, a 20ns MD simulation was carried out

for equilibrium the system. The pull style was chosen as "umbrella", which means

that center of mass pulling using an umbrella potential between the reference group

and the pull group. The pulling geometry of pull code was chosen as "simple", which

is used to pull along the vector connecting the two groups. The Kv1.3 channel was

chosen as reference group and toxin is chosen as pull group. The Z dimension, which

provides a binding pathway between the Kv1.3 channel and the toxins, was chosen as

the reaction coordinate and note that the COM of the channel backbone is at z = 0 Å.

A harmonic force constant of 2000 $KJ \cdot mol^{-1} \cdot nm^{-2}$ was applied at the center of mass

along the Z dimension. At the process of pulling, the pulling rate was set to 0.005

$nm \cdot ps^{-1}$. When simulate each umbrella sample window, the pulling rate was set to

zero which means the harmonic force only maintain the relative position of toxin and

Kv1.3 channel. Along the reaction coordinate, windows are separated at 0.5 Å. Each

umbrella window was simulated for 10 ns to ensure good convergence.

3.Results and discussion

3.1 Toxin structures and docking structures.

We listed five amino acid sequences of α-KTX-3 toxins and their 3-D structures

in **Figure 1**. BmKTX(PDB ID: 1BKT),OSK1(PDB ID:2CK4),AgTX2(PDB ID:

1AGT),KTX(PDB ID: 2UVS).For α-KTX-3 family , they all most have similar

secondary structure, especially , one α-helix formed by L(I)-K-P-C-K-D-A and a pair

conserved anti-parallel β-sheets which formed by G-K-C and C-H(D)-C. The

conserved residue Lys26 and the residue His33(or Asp33) locates at the couple of anti-parallel β-sheets, respectively, and their main chain maintains the stability of the couple of anti-parallel β-sheets by forming two stable hydrogen bonds. Aligning with the amino acid sequence, BmKTX and BmKTX-D33H only has one different No.33 residue: the Asp33 in BmKTX and His33 in BmKTX-D33H, respectively, but the two peptides have two different binding abilities toward to Kv1.3 channel. So, we studied the binding mechanisms of BmKTX-Kv1.3 and [BmKTX-D33H]-Kv1.3 using MD simulation.

To assess the structural stability of the two bind models, we analyzed the time evolution of the root-mean square deviation (RMSD) of CA atoms with respect to the initial structure of BmKTX-Kv1.3 and [BmKTX-D33H]-Kv1.3 in the simulations. In the **Figure 2**, the plots of RMSD became smooth in 20ns simulations and the values of RMSD around a value of 2-2.5 Å after an initial ramping equilibrates, indicating the initial structures had changed a lot after 20ns simulations. Aimed to observe the conformational transformation, we extracted the trajectory information per 50ps and compared the final simulated structures to the initial structures in the **Figure 3**. The tower loop domains of Kv1.3 are very flexible and the transmembrane helix region of Kv1.3 are very stable in the simulations. The toxins' final simulated position change greatly comparing with the initial position and the toxins get closer to Kv1.3 channel with the simulated time increasing, and the secondary structures of BmKTX and BmKTX-D33H both are stable during the process. Overall, the Kv1.3 channel shows

strong attraction for BmKTX and BmKTX-D33H and formed two different binding modes with the two peptides.

The two final simulated binding models refined by 20ns MD are shown in **Figure 4**. BmKTX and BmKTX-D33H shown respectively two different binding models toward to Kv1.3 channel and their interaction surfaces vary greatly. From the top view, the orientations of BmKTX and BmKTX-D33H vary greatly too. Especially, the anti-parallel β-sheet domain of BmKTX was close to the tower loop region of Kv1.3 channel and the anti-parallel β-sheet domain of BmKTX-D33H was close to the filter region of Kv1.3 channel. The residue Asp33 in BmKTX and His33 in BmKTX-D33H were also marked in Figure 3, which located at one of anti-parallel β-sheets and form the hydrogen bond with the conserved Lys26. The two bind models have a same characteristic that conserved basic residues formed hydrogen bonds with Kv1.3 channel which anchor the toxin peptides to the Kv1.3 channel. For BmKTX, the sidechain of conserved Arg23 inserts into the filter region of Kv1.3 channel and forms hydrogen bonds with the oxygen atom of the G446:A,G466:D,Y447:A ,Y447:C ; the sidechain of Lys26 contacts with the outer vestibule region of Kv1.3 channel and forms hydrogen bonds with the main-chain oxygen atom of E420:B,H451:B. For BmKTX-D33H, the sidechain of Arg23 interacts with the outer vestibule region of Kv1.3 channel and forms hydrogen bonds with main-chain oxygen atom of S423:B, P424:B ; the sidechain of Lys26 inserts into the filter region of Kv1.3 channel and forms hydrogen bonds with mainchain oxygen

atom of Y477:A,Y477:B,Y477:C. Detailed interactions were listed in **Table 1** and

Table 2, and we measured the interaction distance between related atoms. The most of

interactions are hydrogen bond interactions between toxin peptides and Kv1.3 channel,

except for Pro24 of BmKTX (or BmKTX-D33H) contacts with Kv1.3 channel using

hydrophobic interaction.

3.2 Umbrella sampling simulations

Umbrella sampling simulation is a common method of calculating binding free

energy (G_b)for toxin-channel complexes[22, 36-38] . In order to determine the reliability of

the docking model, the PMF profiles of the two binding models are calculated. The

binding free energy can be calculated by integrating the PMF, W(z), along the z-axis:

$$K_{eq} = \pi R^2 \int_{z1}^{z2} e^{[-W(z)/k_B T]} dz$$

$$G_b = -k_B T ln(K_{eq} C_0)$$

Where πR^2 is the average cross-sectional area of the binding pocket, z1 and z2

are the initial and final points in the PMF, respectively. C_0 is the standard

concentration of 1 M. The R values has been calculated, which are 0.5 Å of

BmKTX-Kv1.3 binding model and 0.62 Å of BmKTX-D33H-Kv1.3 binding model

respectively.

According to the data from the profiles of PMF, we calculated the G_b of the

BmKTX-Kv1.3 model and the BmKTX-D33H-Kv1.3 model. The G_{b1} and G_{b2} are

used to represent standard binding free energy of BmKXT-Kv1.3 and

[BmKTX-D33H]-Kv1.3. The values of G_{b1} and G_{b2}, are -27 kcal·mol^{-1} and -34kcal·mol^{-1}, respectively, which are consistent with experimental results[18]. It means that BmKTX-D33H has stronger binding than that of BmKTX. Umbrella sampling simulations also provide a wealth of data of the binding process, which can be used to gain further insight into the binding mechanism[39].

Based on above simulation results, hydrogen bond interactions are the main forces to maintain the association of toxin peptides and channels. In this case, we regard hydrogen bonds as anchor points for binding process when toxin peptides binding to Kv.1.3 channel. To describe the binding mechanism, we calculated the average N–O distance between the donors and the acceptors using the data from umbrella sample windows. When the N-O distance exceeds 5 Å, hydrogen bond is hardly existed. In the Figure 5-a and 5-b, at the 32 Å of reaction coordinate, the PMF profile of BmKTX-Kv1.3 became smooth and the anchor(R23-Y447:A) was destroyed. In the Figure 5-c and 5-d, at the 36 Å of reaction coordinate, the PMF profile of [BmKTX-D33H]-Kv1.3 became smooth and the anchor(R23-P424:B) was destroyed. Above all, along reaction coordinate, toxin peptides and Kv.13 channel were in three states: the bound state, partially bound state and unbound state. For BmKTX, at 25 Å of reaction coordinate, BmKTX-Kv1.3 was in the bound state; from 25 Å to 32 Å of reaction coordinate, BmKTX-Kv1.3 was in the partially bound state; beyond 32 Å of reaction coordinate, BmKTX-Kv1.3 was in the unbound state. For BmKTX-D33H, at 26 Å of reaction coordinate, [BmKTX-D33H]-Kv1.3 was in the

bound state; from 26 Å to 36 Å of reaction coordinate, [BmKTX-D33H]-Kv1.3 was in the partially bound state; beyond 36 Å of reaction coordinate, [BmKTX-D33H]-Kv1.3 was in the unbound state. From the unbound state to the fully bound state, toxin peptide would constantly adjust its orientation until make a stable bound state with Kv1.3 channel. On the binding process, the different No.33 residue of α-KTX-3 toxins do not interact with the Kv1.3 channel, but it determined the final binding model of toxin-Kv1.3 channel. For BmKTX, the conserved Lys26 keep away from the filter region of Kv1.3 channel and the sidechain of Arg23 finally block the filter region of Kv1.3 channel and; for BmKTX-D33H, Arg23 interact with the tower region of Kv1.3 channel and the sidechain of Lys26 in BmKTX-D33H finally block the filter region of Kv1.3 channel Arg23 close to the filter region of Kv1.3 channel. In addition, the [BmKTX-D33H]-Kv1.3 docking model have stronger binding affinity than that of BmKTX-Kv1.3 docking model according to the PMF profiles. From the above data, we verified that the two different binding models are trusted and obtained the atomic details of the two different binding process using umbrella sample simulation.

3.3 Electrostatic potential and cross-correlation

The APBS 1.5[40] was used to map the electrostatic potential of the toxins and the Kv1.3 channel . The negative charge is rich in the filter region of Kv1.3 channel, because it is formed by amino acid residues T-V-G-Y-G-D and their oxygen atoms were exposed to the outside (shown in **Figure 6**). Therefore, the filter region of Kv1.3

will attract the object with positive charge and repulse the object with negative charge. And that, BmKTX and BmKTX-D33H have a different charged residue in No.33 of amino acid sequence and produce an obvious difference of electrostatic potential around the molecular surface (shown in **Figure 7**)**.** For BmKTX, the region around the Asp33 will be repulsed by the filter region of Kv1.3 channel. For BmKTX-D33H, His33 improved the positive electrostatic potential; therefore, the region around the His33 will easily reach the filter region of Kv1.3 channel. It is noteworthy that the Asp33 of BmKTX (or His33 of BmKYX-D33H) and conserved Lys26 formed two stable hydrogen bonds on the backbone, that means conserved Lys26 must be influenced by No.33 residue in the two toxins.

In the α-KTX-3 family, the residue 26(27) and residue 33(34) severally locates at a pair of anti-parallel β-sheets and formed two stable hydrogen bonds on the backbone. Here, we ran 100ns simulations for α-KTX-3 toxins sampled as BmKTX, BmKTX-D33, KTX and AgTX2 to examine the motion correlation of residues. We analyzed these trajectories by Bio3D[41] R package. The residue cross correlations are showed in the **Figure 8** and the visualized data are showed in the **Figure 9**. Note that, residue cross correlation coefficients of conserved anti-parallel β-sheet domain(formed by G-K-C and C-H(D)-C) was listed in **Table 3** .We found that residue33(34) and the conserved Lys26(27) have positive motion correlation in the four α-KTX-3 toxins. It means that the anti-parallel β-sheet domain is stable and will motion consistently. Especially, for BmKTX, the anti-parallel β-sheet domains will

keep away from the filter region of Kv1.3 channel, because the region around the Asp33 will be repulsed by the filter region of Kv1.3 channel. However, for BmKTX-D33H(or KTX,AgTX2), the anti-parallel β-sheet domains will be attracted to the filter region of Kv1.3 channel and the sidechain of conserved Lys27 will block the filter region of Kv1.3 channel. Therefore, BmKTX has a different binding model toward to Kv1.3 channel comparing with the other α-KTX-3 toxins. These observations provide insights into the mechanisms of acidic residue adjusting the toxin- potassium channel binding model.

4.Conclusion

We studied the BmKTX-Kv1.3 and [BmKTX-D33H]-Kv1.3 binding mechanism using MD simulation and umbrella sampling simulation. Two reliable binding models of BmKTX-Kv1.3 and [BmKTX-D33H]-Kv1.3, and hydrogen bonds paly key important role in the α-KTX-3 toxin-Kv1.3 channel binding process and the characteristic of electrostatic potential of the α-KTX-3 toxins will adjust the binding orientations toward to Kv1.3 channel. And that, the residue 33(34) is an decisive factor for adjusting the anti-parallel β-sheet domain of α-KTX-3 toxins position relative to Kv1.3 channel, due to the stronger positive motion correlation with conserved Lys26(27) of α-KTX-3 toxins. As a consequence, BmKTX and BmKTX-D33H make have different binding models toward to Kv1.3 channel. Diverse toxin–potassium channel binding modes often means a variety of drug effects, BmKTX-D33H have stronger binding affinity toward to Kv1.3 channel than wild BmKTX. The binding mechanism in the paper will facilitate the discovery of the accurate toxin-potassium binding model and the therapeutic potential of toxin-peptides.

.

References

1. Beeton, C.; Chandy, K. G., Potassium channels, memory T cells, and multiple sclerosis. *Neuroscientist* **2005,** *11* (6), 550-62.

2. Wulff, H.; Calabresi, P. A.; Allie, R.; Yun, S.; Pennington, M.; Beeton, C.; Chandy, K. G., The voltage-gated Kv1.3 K(+) channel in effector memory T cells as new target for MS. *J Clin Invest* **2003,** *111* (11), 1703-13.

3. Lam, J.; Wulff, H., The Lymphocyte Potassium Channels Kv1.3 and KCa3.1 as Targets for Immunosuppression. *Drug Dev Res* **2011,** *72* (7), 573-584.

4. Gulbins, E.; Sassi, N.; Grassme, H.; Zoratti, M.; Szabo, I., Role of Kv1.3 mitochondrial potassium channel in apoptotic signalling in lymphocytes. *Biochim Biophys Acta* **2010,** *1797* (6-7), 1251-9.

5. Kalman, K.; Pennington, M. W.; Lanigan, M. D.; Nguyen, A.; Rauer, H.; Mahnir, V.; Paschetto, K.; Kem, W. R.; Grissmer, S.; Gutman, G. A.; Christian, E. P.; Cahalan, M. D.; Norton, R. S.; Chandy, K. G., ShK-Dap22, a potent Kv1.3-specific immunosuppressive polypeptide. *J Biol Chem* **1998,** *273* (49), 32697-32707.

6. Schmitz, A.; Sankaranarayanan, A.; Azam, P.; Schmidt-Lassen, K.; Homerick, D.; Hänsel, W.; Wulff, H., Design of PAP-1, a Selective Small Molecule Kv1.3 Blocker, for the Suppression of Effector Memory T Cells in Autoimmune Diseases. *Molecular Pharmacology* **2005,** *68* (5), 1254.

7. Ye, F.; Hu, Y.; Yu, W.; Xie, Z.; Hu, J.; Cao, Z.; Li, W.; Wu, Y., The Scorpion Toxin Analogue BmKTX-D33H as a Potential Kv1.3 Channel-Selective Immunomodulator for Autoimmune Diseases. *Toxins* **2016,** *8* (4).

8. Koo, G. C.; Blake, J. T.; Talento, A.; Nguyen, M.; Lin, S.; Sirotina, A.; Shah, K.; Mulvany, K.; Hora, D.; Cunningham, P.; Wunderler, D. L.; McManus, O. B.; Slaughter, R.; Bugianesi, R.; Felix, J.; Garcia, M.; Williamson, J.; Kaczorowski, G.; Sigal, N. H.; Springer, M. S.; Feeney, W., Blockade of the voltage-gated potassium channel Kv1.3 inhibits immune responses in vivo. *The Journal of Immunology* **1997,** *158* (11), 5120.

9. Giangiacomo, K. M.; Ceralde, Y.; Mullmann, T. J., Molecular basis of alpha-KTx specificity. *Toxicon* **2004,** *43* (8), 877-86.

10. Gwee, M. C. E.; Nirthanan, S.; Khoo, H.-E.; Gopalakrishnakone, P.; Kini, R. M.; Cheah, L.-S., Autonomic effects of some scorpion venoms and toxins. *Clinical and Experimental Pharmacology and Physiology* **2002,** *29* (9), 795-801.

11. Possani, L. D.; Merino, E.; Corona, M.; Bolivar, F.; Becerril, B., Peptides and genes coding for scorpion toxins that affect ion-channels. *Biochimie* **2000,** *82* (9), 861-868.

12. Tytgat, J.; Chandy, K. G.; Garcia, M. L.; Gutman, G. A.; Martin-Eauclaire, M.-F.; van der Walt, J. J.; Possani, L. D., A unified nomenclature for short-chain peptides isolated from scorpion venoms: α-KTx molecular subfamilies. *Trends in Pharmacological Sciences* **1999,** *20* (11), 444-447.

13. Martin-Eauclaire, M. F.; Bougis, P. E., Potassium Channels Blockers from the Venom of Androctonus mauretanicus mauretanicus. *J Toxicol* **2012,** *2012*, 103608.

14. Chen, R.; Robinson, A.; Gordon, D.; Chung, S. H., Modeling the binding of three toxins to the voltage-gated potassium channel (Kv1.3). *Biophys J* **2011,** *101* (11), 2652-60.

15. Mouhat, S.; Visan, V.; Ananthakrishnan, S.; Wulff, H.; Andreotti, N.; Grissmer, S.; Darbon, H.; De Waard, M.; Sabatier, J.-M., K<sup>+</sup> channel types targeted by synthetic OSK1, a toxin from Orthochirus scrobiculosus scorpion venom. *Biochemical Journal* **2005,** *385* (1), 95.

16. Eriksson, M. A. L.; Roux, B., Modeling the Structure of Agitoxin in Complex with the Shaker K+ Channel: A Computational Approach Based on Experimental Distance Restraints Extracted from Thermodynamic Mutant Cycles. *Biophysical Journal* **2002,** *83* (5), 2595-2609.

17. Mourre, C.; Chernova, M. N.; Martin-Eauclaire, M.-F.; Bessone, R.; Jacquet, G.; Gola, M.; Alper, S. L.; Crest, M., Distribution in Rat Brain of Binding Sites of Kaliotoxin, a Blocker of Kv1.1 and Kv1.3 α-Subunits. *Journal of Pharmacology and Experimental Therapeutics* **1999,** *291* (3), 943.

18. Chen, Z.; Hu, Y.; Hu, J.; Yang, W.; Sabatier, J. M.; De Waard, M.; Cao, Z.; Li, W.; Han, S.; Wu, Y., Unusual binding mode of scorpion toxin BmKTX onto potassium channels relies on its distribution of acidic residues. *Biochem Biophys Res Commun* **2014,** *447* (1), 70-6.

19. Chen, R.; Tong, W.; Mintseris, J.; Li, L.; Weng, Z., ZDOCK predictions for the CAPRI challenge. *Proteins: Structure, Function, and Bioinformatics* **2003,** *52* (1), 68-73.

20. Quintero-Hernandez, V.; Jimenez-Vargas, J. M.; Gurrola, G. B.; Valdivia, H. H.; Possani, L. D., Scorpion venom components that affect ion-channels function. *Toxicon* **2013,** *76*, 328-42.

21. Bhuyan, R.; Seal, A., Molecular dynamics of Kv1.3 ion channel and structural basis of its inhibition by scorpion toxin-OSK1 derivatives. *Biophys Chem* **2015,** *203-204*, 1-11.

22. Deplazes, E., Molecular Simulations of Disulfide-Rich Venom Peptides with Ion Channels and Membranes. *Molecules* **2017,** *22* (3).

23. Li, D.; Chen, R.; Chung, S. H., Molecular dynamics of the honey bee toxin tertiapin binding to Kir3.2. *Biophys Chem* **2016,** *219*, 43-48.

24. Mahdavi, S.; Kuyucak, S., Molecular dynamics study of binding of micro-conotoxin GIIIA to the voltage-gated sodium channel Na(v)1.4. *PLoS One* **2014,** *9* (8), e105300.

25. Zachariae, U.; Schneider, R.; Velisetty, P.; Lange, A.; Seeliger, D.; Wacker, S. J.; Karimi-Nejad, Y.; Vriend, G.; Becker, S.; Pongs, O.; Baldus, M.; de Groot, B. L., The molecular mechanism of toxin-induced conformational changes in a potassium channel: relation to C-type inactivation. *Structure* **2008,** *16* (5), 747-54.

26. Waterhouse, A.; Bertoni, M.; Bienert, S.; Studer, G.; Tauriello, G.; Gumienny, R.; Heer, F. T.; de Beer, T. A P.; Rempfer, C.; Bordoli, L.; Lepore, R.; Schwede, T., SWISS-MODEL: homology modelling of protein structures and complexes. *Nucleic Acids Research* **2018,** *46* (W1), W296-W303.

27. Waterhouse, A.; Bertoni, M.; Bienert, S.; Studer, G.; Tauriello, G.; Gumienny, R.; Heer, F. T.; de Beer, T. A. P.; Rempfer, C.; Bordoli, L.; Lepore, R.; Schwede, T., SWISS-MODEL: homology modelling of protein structures and complexes. *Nucleic Acids Res* **2018,** *46* (W1), W296-W303.

28. van Zundert, G. C. P.; Rodrigues, J.; Trellet, M.; Schmitz, C.; Kastritis, P. L.; Karaca, E.; Melquiond, A. S. J.; van Dijk, M.; de Vries, S. J.; Bonvin, A., The HADDOCK2.2 Web Server: User-Friendly Integrative Modeling of Biomolecular Complexes. *J Mol Biol* **2016,** *428* (4), 720-725.

29. Abraham, M. J.; Murtola, T.; Schulz, R.; Páll, S.; Smith, J. C.; Hess, B.; Lindahl, E., GROMACS: High performance molecular simulations through multi-level parallelism from laptops to supercomputers. *SoftwareX* **2015,** *1-2*, 19-25.

30. Oostenbrink, C.; Villa, A.; Mark, A. E.; Van Gunsteren, W. F., A biomolecular force field based on the free enthalpy of hydration and solvation: The GROMOS force-field parameter sets 53A5 and 53A6. *Journal of Computational Chemistry* **2004,** *25* (13), 1656-1676.

31. Miyamoto, S.; Kollman, P. A., Settle: An analytical version of the SHAKE and RATTLE algorithm for rigid water models. *Journal of Computational Chemistry* **1992,** *13* (8), 952-962.

32. Jójárt, B.; Martinek, T. A., Performance of the general amber force field in modeling aqueous POPC membrane bilayers. *Journal of Computational Chemistry* **2007,** *28* (12), 2051-2058.

33. Evans, D. J.; Holian, B. L., The Nose–Hoover thermostat. *The Journal of Chemical Physics* **1985,** *83* (8), 4069-4074.

34. Melchionna, S.; Ciccotti, G.; Lee Holian, B., Hoover NPT dynamics for systems varying in shape and size. *Molecular Physics* **1993,** *78* (3), 533-544.

35. Kumar, S.; Rosenberg, J. M.; Bouzida, D.; Swendsen, R. H.; Kollman, P. A., THE weighted histogram analysis method for free-energy calculations on biomolecules. I. The method. *Journal of Computational Chemistry* **1992,** *13* (8), 1011-1021.

36. Kästner, J., Umbrella sampling. *Wiley Interdisciplinary Reviews: Computational Molecular Science* **2011,** *1* (6), 932-942.

37. Heinzelmann, G.; Chen, P. C.; Kuyucak, S., Computation of standard binding free energies of polar and charged ligands to the glutamate receptor GluA2. *J Phys Chem B* **2014,** *118* (7), 1813-24.

38. Rashid, M. H.; Kuyucak, S., Free energy simulations of binding of HsTx1 toxin to Kv1 potassium channels: the basis of Kv1.3/Kv1.1 selectivity. *J Phys Chem B* **2014,** *118* (3), 707-16.

39. Chen, P. C.; Kuyucak, S., Mechanism and energetics of charybdotoxin unbinding from a potassium channel from molecular dynamics simulations. *Biophys J* **2009,** *96* (7), 2577-88.

40. Baker, N. A.; Sept, D.; Joseph, S.; Holst, M. J.; McCammon, J. A., Electrostatics of nanosystems: Application to microtubules and the ribosome. *Proceedings of the National Academy of Sciences* **2001,** *98* (18), 10037.

41. Grant, B. J.; Rodrigues, A. P.; ElSawy, K. M.; McCammon, J. A.; Caves, L. S., Bio3d: an R package for the comparative analysis of protein structures. *Bioinformatics* **2006,** *22* (21), 2695-6.

Table

Table 1. Interactions between BmKTX and Kv1.3 channel.

Residue of BmKTX	Residue of Kv1.3	Hydrogen bond(Å)	Hydrophobic(Å)
$K18\text{-}N_Z$	$[G449\text{:}B]\text{-}O$	3.1	-
$K18\text{-}N_Z$	$[G449\text{:}D]\text{-}O$	3.3	-
$R23\text{-}N_E$	$[G447\text{:}A]\text{-}O$	2.9	-
$R23\text{-}N_{H1}$	$[Y447\text{:}C]\text{-}O$	3.1	
$R23\text{-}N_{H1}$	$[G447\text{:}D]\text{-}O$	3.0	-
$R23\text{-}N_{H2}$	$[G446\text{:}C]\text{-}O$	2.9	-
$R23\text{-}N_{H2}$	$[G446\text{:}A]\text{-}O$	3.1	-
$F24\text{-}C_{E2}$	$[H501\text{:}B]\text{-}C_{D2}$	-	3.4
$F24\text{-}C_Z$	$[Y477\text{:}A]\text{-}C_{D1}$	-	3.6
$K26\text{-}N_Z$	$[E420\text{:}B]\text{-}O_{E1}$	3.3	-
$K26\text{-}N_Z$	$[H451\text{:}B]\text{-}O$	2.9	-
$I28\text{-}N$	$[G426\text{:}B]\text{-}O$	3.0	-
$K37\text{-}N_Z$	$[D449\text{:}A]\text{-}O$	3.1	-
$K37\text{-}N_Z$	$[S426\text{:}A]\text{-}O$	2.9	-

Table 2. Interactions between BmKTX-D33H and Kv1.3 channel.

Residue of BmKTX-D33H	Residue of Kv1.3	Hydrogen bond(Å)	Hydrophobic(Å)
$H9\text{-}N_{E2}$	$[D432\text{:}C]\text{-}O_{D2}$	2.7	-
$R23\text{-}N_E$	$[S423\text{:}B]\text{-}O$	3.3	-
$R23\text{-}N_E$	$[P424\text{:}B]\text{-}O$	2.8	-
$R23\text{-}N_{H2}$	$[P424\text{:}B]\text{-}O$	2.8	
$F24\text{-}C_{D1}$	$[H501\text{:}B]\text{-}C_B$	-	3.4
$F24\text{-}C_Z$	$[M500\text{:}B]\text{-}C_G$	-	4.2
$K26\text{-}N_Z$	$[Y477\text{:}A]\text{-}O$	3.1	-
$K26\text{-}N_Z$	$[Y477\text{:}B]\text{-}O$	2.9	-
$K26\text{-}N_Z$	$[Y477\text{:}C]\text{-}O$	3.0	-

Table 3. The residue cross correlation coefficients for conserved anti-parallel β-sheet domain.

BmKTX		C32	D33	C34	BmKTX -D33H		C32	H33	C34
	G25	0.21	0.40	0.39		G25	0.22	0.44	0.43
	K26	0.30	0.57	0.43		K26	0.21	0.52	0.37
	C27	0.32	0.38	0.23		C27	0.05	0.12	0.00
KTX		C33	H34	C35	AgTX2		C32	H34	C35
	G26	0.05	0.21	0.05		G26	-0.01	0.21	0.12
	K27	0.15	0.47	0.11		K27	0.13	0.54	0.13
	C28	0.00	0.12	0.04		C28	-0.01	0.17	0.04

Figure legends

Figure 1. (a) Primary structures of α-KTx-3 toxin family. Note that, on the same No.33 residue position of α-KTx-3 toxins, Asp in BmKTX and His in BmKTX-D33H, His34 of AgTX2(or OSK1, KTX). (b) The 3-D structures of five typical α-KTx-3 toxins are shown. The α-helix is colored by red and the β-sheet is colored by green. The conserved anti-parallel β-sheets which formed by G-K-C and C-H(D)-C and the backbone of residue 26(27) and residue 33(34) formed two stable hydrogen bonds. The conserved Arg23 locate at the turn motif domain between the α-helix domain and anti-parallel β-sheet domain.

Figure 2. Time-evolution of RMSD values respecting to the initial structure of toxin peptide-Kv1.3 complexes.

Figure 3. The conformational changes respecting to the initial structure of toxin peptide-Kv1.3 complexes. The initial structure of Kv1.3 channel was colored by sliver and initial structure of toxin-peptide was colored by pink. The final simulated structure of Kv1.3 channel was blue and the final simulated structure of toxin-peptide was green. (a) The initial structure of BmKTX-Kv1.3 and the final simulated structure of BmKTX-Kv1.3. (b) The conformational changes of BmKTX-Kv1.3 in 20ns MD simulation. (c) The initial structure of [BmKTX-D33H]-Kv1.3 and the final simulated

structure of [BmKTX-D33H]-Kv1.3. (d) the conformational changes of [BmKTX-D33H]-Kv1.3 in 20ns MD simulation.

Figure 4. The binding models of BmKTX-Kv1.3 and [BmKTX-D33H]-Kv1.3 were refined by two 20ns simulations. The interaction surface of Kv1.3 channel was colored by red and the residues of toxin peptides involved in interactions were colored by blue.

Figure 5. PMF profiles and the anchor changes of toxin peptide-Kv1.3 channel. The distance of center of mass between toxin peptides and Kv1.3 channel was made as reaction coordinate.

Figure 6. The electrostatic potential map of the transmembrane region of Kv1.3 channel. Negative electrostatic region was red, positive electrostatic region was blue.

Figure 7. The electrostatic potential maps of toxin-peptides. Negative electrostatic region is colored by red, positive electrostatic region is colored by blue. (a) BmKTX. (b) BmKTX-D33H.

Figure 8. The residue cross correlation of four typical members of α-KTX-3 subfamily. The residue cross correlation coefficients are got from the 100ns
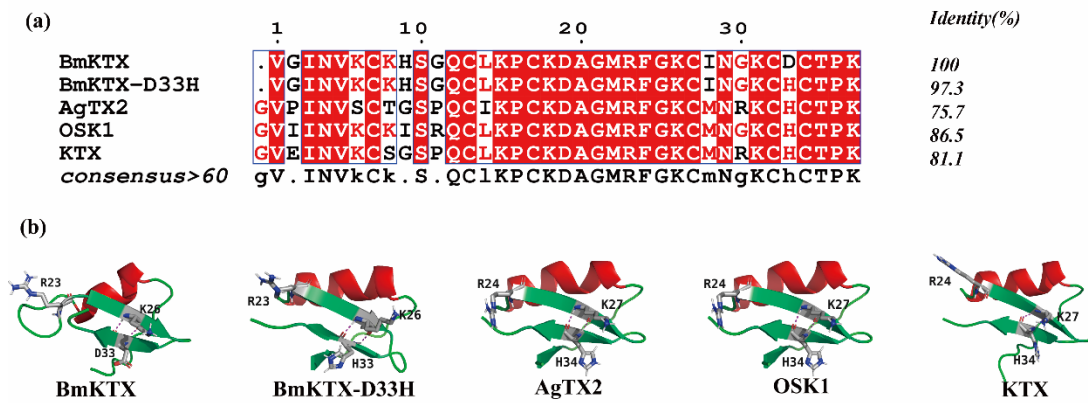
simulation's trajectory files, using Bio3D R package. (a) BmKTX. (b) BmKTX-D33H. (c) KTX. (d) AgTX2. Note that, the intersection of residue 26(27) and residue 33(34) was colored by red, it means they have a stronger positive motion correlation.
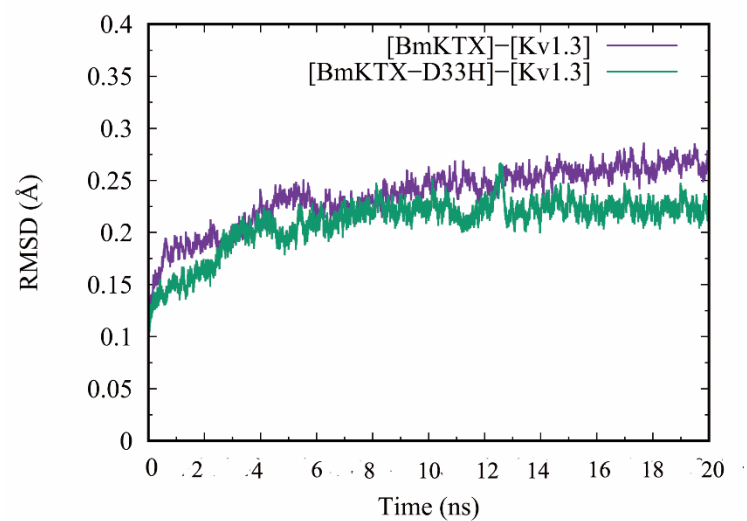
Figure 9. The visualization of residue cross correlation of four α-KTX-3 toxins. (a) BmKTX, (b) BmKTX-D33H, (c) KTX, (d) AgTX2. Note that, red lines signify positive correlation between the two residues and blue lines signify negative correlation between the two residues.

Figures
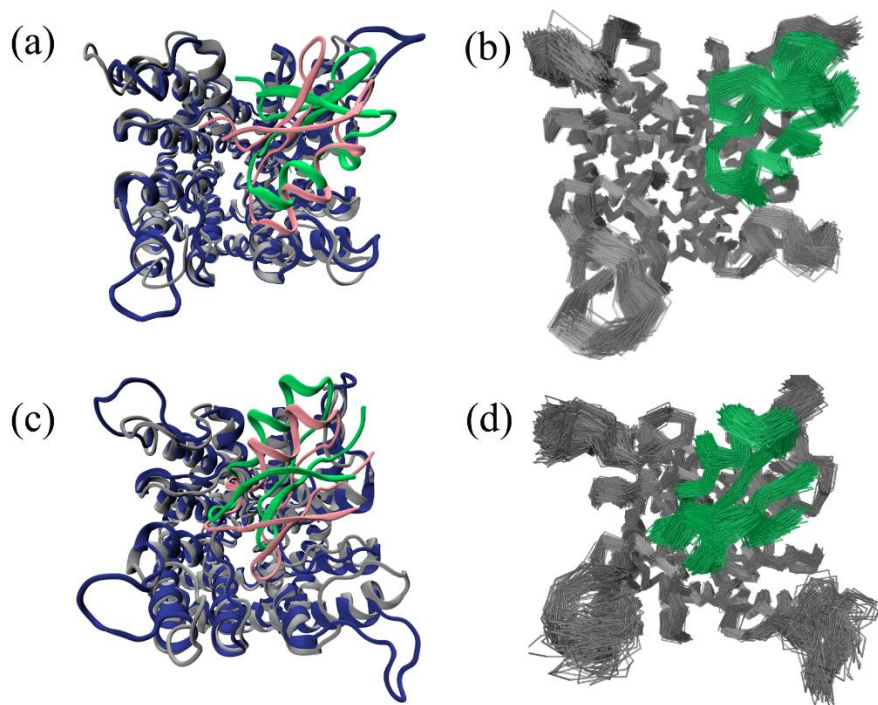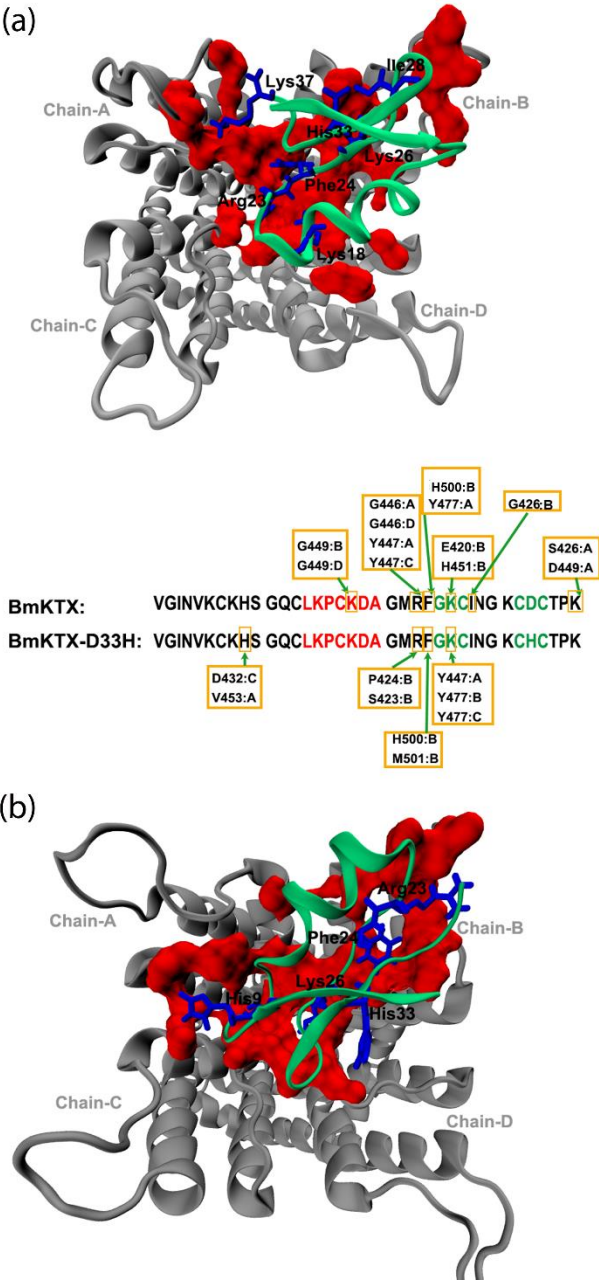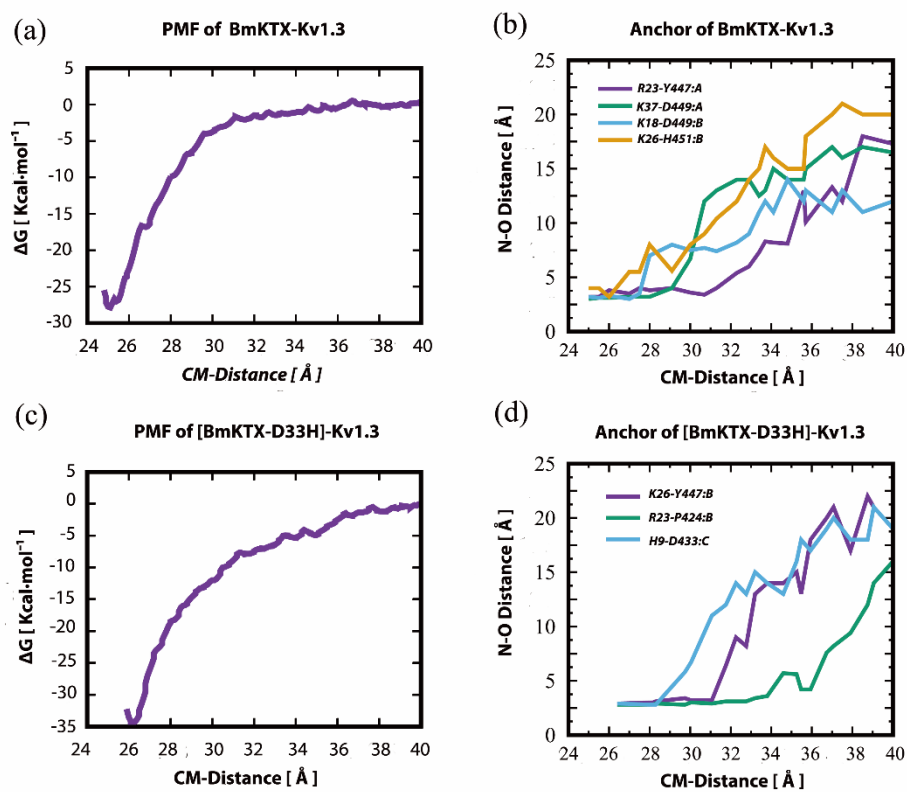
Figure 1
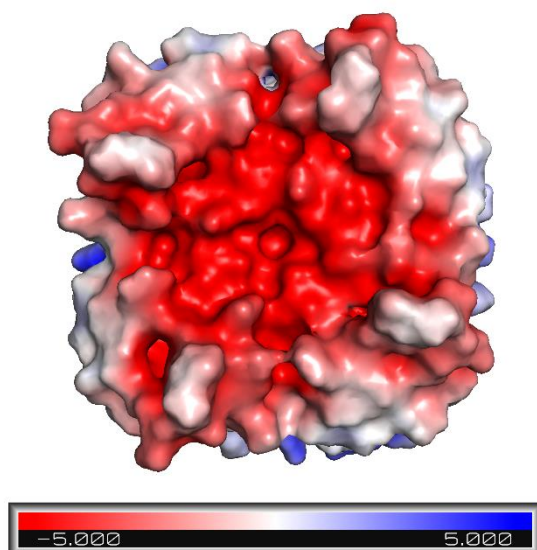
Figure 2.

Figure 3.

Figure 4.

BmKTX: VGINVKCKHS GQCLKPCKDA GMRFGKCING KCDCTPK

BmKTX-D33H: VGINVKCKHS GQCLKPCKDA GMRFGKCING KCHCTPK

Figure 5.

Figure 6.

Figure 7.

(a)   (b)

Figure 8.

(a)

(b)

(c)

(d)

Figure 9.

(a) BmKTX

(b) BmKTX-D33H

(c) KTX

(d) AgTX2